WARSAW UNIVERSITY OF TECHNOLOGY Index 351733
FACULTY OF CIVIL ENGINEERING
COMMITTEE FOR CIVIL AND WATER ENGINEERING
POLISH ACADEMY OF SCIENCES ISSN 1230-2945

DOI: 10.24425/ace.2020.136477

ARCHIVES OF CIVIL ENGINEERING

Vol. LXVII ISSUE 1 2021

ANALYSIS OF TEMPERATURE-FIELD AND STRESS-FIELD OF STEEL PLATE CONCRETE COMPOSITE SHEAR WALL IN EARLY STAGE OF CONSTRUCTION

YUN SUN[1], YAOJIE GUO[2]

Abstract: To study the influence of temperature field and stress field on the cracking of the small thickness steel plate concrete composite shear wall (SPCW) in the early stage of construction. The temperature field and stress field of a 400 mm thickness SPCW was monitored and simulated through experimental research and numerical simulation. Moreover, a series of parameter analyses were carried out by using ANSYS to investigate the distribution of temperature field and stress field of SPCW. Based on the analysis results, some suggestions are put forward for controlling the cracking of SPCW in the early stage of construction. The results show that the temperature stress of 400 mm thickness SPCW in the early stage of construction is small, and there is no crack on the wall surface. For SPCW with thickness less than 800mm, the temperature stress caused by hydration heat in the early stage of construction is small, and the wall will not crack. The parameters such as wall thickness, steel plate thickness, boundary condition and stud space significantly influence the temperature field and stress field distribution of the small thickness SPCW in the early stage of construction, and reasonable maintenance measures can avoid cracking.

*Keywords***:** steel plate concrete composite shear wall; temperature field; stress field; thermal analysis; cracking

[1] PhD., Wuhan University, School of Civil Engineering, No.8 of Donghu South Road in Wuhan, Hubei, China, e-mail: sunyun@whu.edu.cn

[2] Prof., PhD., Wuhan University, School of Civil Engineering, No.8 of Donghu South Road in Wuhan, Hubei, China, e-mail: whuguoyaojie@163.com

1. INTRODUCTION

Steel plate concrete composite shear wall (SPCW) has widely used in super high-rise buildings because of its high lateral stiffness, excellent bearing performance, and the convenience of construction [1-2]. The representative projects include the Nippon Steel Building (1970) and Shinjuku Nomura Office Tower (1978) in Japan, Sylmar County Hospital (1971), and Federal Courthouse (2004) in the USA, Jin Jiang Tower Shanghai (1987) and Wuhan Center (2015) in China. Compared to the conventional reinforced concrete shear wall, SPCW consists of high-performance concrete, embedded steel plates, and densely distributed studs that have better mechanical performance. Research on the bearing capacity and seismic performance of SPCW has obtained lots of achievements [3-6]. In the early stage of construction, the high-performance concrete produces hydration heat in a short time and accumulates much heat. The uneven heat dissipation will create temperature stress. Under the steel plate and bolt's combined restraint action, the SPCW is liable to crack by temperature stress, which affected its durability. Therefore, the crack problem of the SPCW caused by the temperature stress in the early stage of construction seems to be the critical problem that perplexes the constructors.

Several researchers are concerned about SPCW cracking causes in the early stage of construction and obtained many useful results. The influence of reinforcement on SPCW shrinkage was analyzed by Yoo et al. [7-8]. Zeng [9] analyzed the influence of stud on the cracking of SPCW by numerical simulation method and obtained the highest cracking potential of concrete being pinpointed as near the studs. Huang [10-11] analyzed the influence of steel plates and studs on the cracking potential of SPCW and demonstrated that the concrete near steel plate and stud is prone to crack. However, these studies analyzed individual components' role in SPCW during cracking and did not involve the various components' combined effects. The factor of influence about cracking of large SPCW was studied by YE et al. [12], in which the hydration heat, moulding temperature, coefficient of heat transfer, and steel ratio on cracking of SPCW were discussed. Some measures to alleviate the temperature stress of concrete in the early stage of construction were put forward by Gu [13].

In summary, these studies are based on the specific analysis of the actual project to guide the engineering design, and all of the walls are more than 800mm, which belongs to the category of large thickness concrete. Meanwhile, in our previous engineering experience, only 400mm thickness SPCW was used in Fanhai International Town in WuHan, but there appeared a large cracking area in the early stage of construction. However, the relevant design specifications and research do not have enough evidence or solution providers to explain this phenomenon. Moreover, we will start a new

project in which the thickness of SPCW is 400 mm~ 600 mm (less than 800mm). Therefore, this study investigates the influence of temperature field and stress field on cracking the small thickness (less than 800mm) SPCW in the early stage of construction to help designers develop solutions to overcome cracking. The temperature field and stress field of a typical SPCW with 400 mm thickness were tested. Numerical analysis of temperature field and stress field with small thickness SPCW were then carried out through ANSYS. The influence rules with different parameters such as wall thickness, boundary condition, steel plate thickness and stud space on cracking were summarized. Finally, the maintenance measures to prevent small thickness SPCW cracking caused by temperature stress at the early stage of construction were put forward.

2. EXPERIMENTAL INVESTIGATION

2.1. EXPERIMENT DESIGN

The building area of Fanyue Town project in Wuhan of China is 635720mm^2, and the thickness of SPCW ranges from 400 mm to 600 mm. In order to understand the effect of hydration heat on SPCW cracking, the temperature field and stress field were studied before the construction. Base on the test site condition and reduce the test difficulty, only a 4000mm×3500mm×400mm SPCW was selected as the specimen. The schematic of the specimen is shown in Fig. 1.

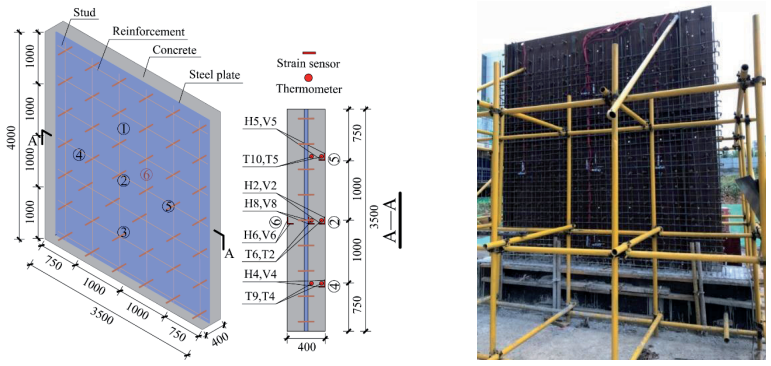

(a) schematic of test wall (b) SPCW before pouring

Fig. 1. The test SPCW

The steel plate thickness is 15mm, and the yield strength is 345MPa. The stud length is 150 mm, the diameter is 20 mm, and the spacing is 300 mm. The reinforcement diameter is Φ18, the tied reinforcement diameter is Φ6, and the reinforcement spacing is 150 mm. The C60 concrete prepared according to the 28d design strength was used. The slump of concrete was measured before pouring to ensure that it can meet the construction requirement. The test was carried out in August with a high atmosphere temperature, which belongs to summer construction. The specimen pouring time was selected after 5:00 PM to avoiding the day's high-temperature time. Moreover, the molding temperature of concrete should be less than 30 °C to reduce the influence on cracking. After pouring, the specimen should be covered and moisturized, and the water should be sprinkled in time to keep the specimen stay in a wet state.

The boundary conditions are mainly imposed by the convection coefficient and the atmosphere temperature on the SPCW surface during the temperature field analysis. There are two kinds of constraint forms of SPCW, i.e., two-side connection and four-side connection in the stress field. The two-side connection means that the wall is connected with the frame beam, and the degrees of freedom (DOF) of the wall top and bottom surfaces are constrained. The four-side connection means that the wall is connected with the frame beam and column, i.e., the DOF of the wall four surfaces (top, bottom, left, and right) are constrained. The specimen bottom is connected with the foundation; the left and right sides are connected with concealed columns. Due to the limitation of test conditions, there are no beams and plates on the wall, which lead the top surface is free. In other words, the DOF of the specimen surfaces are constrained except for the top surface. The specimen can still reflect the change rule of the actual component's temperature field and stress field to some extent. The discussion on the effects of two-side connection or four-side connection boundary conditions on the SPCW is described in section 4 below.

The FY-EJ61 concrete strain sensors and thermometers were used to monitor the temperature field and stress field variation. The DH3815N strain box and M400 multi-channel temperature data logger are used to collect strain data and temperature data, respectively. Due to the symmetry of the wall, five measuring points arranged on one side of the specimen. Along the specimen's vertical central axis, three points marked as ①, ② and ③ are arranged at equal intervals (1 m). Along the specimen's horizontal central axis with ② as the midpoint, the interval is 1 m, and one point on each of the left and right sides respectively marked as ④ and ⑤. On the other side of the specimen, arrange a point at the centre marked as ⑥. The layout of points is shown in Fig. 1. At ①~⑤ points, five thermometers are arranged at specimen external numbered T1~T5, and five thermometers are arranged at specimen internal numbered T6~T10. At ①~⑥ point, six strain sensors are arranged at horizontal direction of

specimen external numbered H1~H6, and six strain sensors are arranged at vertical direction of specimen external numbered V1~V6. Furthermore, at ①~③ points, three strain sensors are arranged at the horizontal direction of specimen internal numbered H7~H9, and three strain sensors are arranged at the vertical direction of specimen internal numbered V7~V9. The number of strain sensors and thermometers are shown in Table 1.

Table 1. The number of strain sensors and thermometers

Measuring point			①	②	③	④	⑤	⑥
Thermometers	external		T1	T2	T3	T4	T5	/
	internal		T6	T7	T8	T9	T10	/
Strain sensors	external	horizontal	H1	H2	H3	H4	H5	H6
		vertical	V1	V2	V3	V4	V5	V6
	internal	horizontal	H7	H8	H9	/	/	/
		vertical	V7	V8	V9	/	/	/

Tips: "/" indicates that no thermometer or strain sensor arranged at this point. There are 10 thermometers and 18 strain sensors in total.

2.2. EXPERIMENT RESULTS AND ANALYSIS

The temperature data are collected every half an hour, and the monitoring time lasted 120 h. The temperature-time curves of each point are shown in Fig. 2.

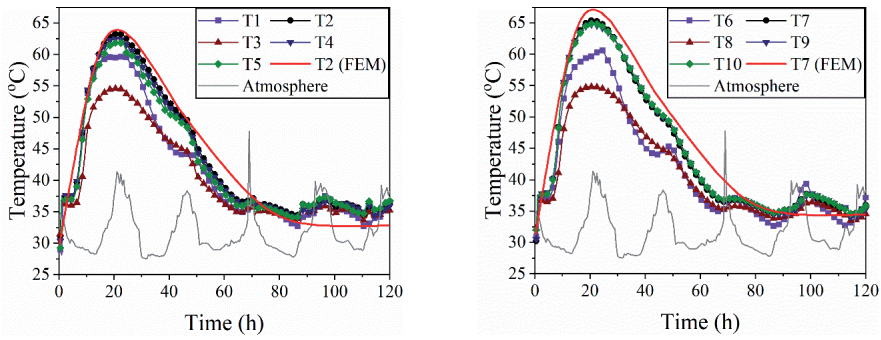

(a) external (b) internal

Fig. 2. Temperature-time curve of specimen

It can see that the temperature changes trend with time at each point is very similar. The temperature-time curve can be divided into three stages. In Stage I (0 h~21.5 h), the hydration heat is released quickly, which causes the temperature to rise rapidly. Whether specimen external or specimen internal, the region of maximum temperature is located at the centre. The specimen's temperature reaches the maximum at 21.5 h. The maximum temperature value on the specimen external is 62.9 ^{o}C, and the specimen internal is 65.8 ^{o}C. The reasons for the temperature difference between external and internal are as follows. On the one hand, there is no contact between the specimen internal and the atmosphere. The heat of specimen internal is mainly transferred to the steel plate and bolt, which leads to slow heat dissipation. On the other hand, the specimen external can exchange heat convection directly with the atmosphere to increase dissipation heat speed and then lose more heat. In stage II (21.5 h~70 h), with the hydration heat is released, the temperature begins to drop rapidly. In stage III (70 h~120 h), the temperature difference between external and internal became small with the heat dissipation, and the specimen temperature is close to the atmosphere.

The strain-time curve of each point is shown in Fig. 3. The tensile strain is positive, and the compressive strain is negative.

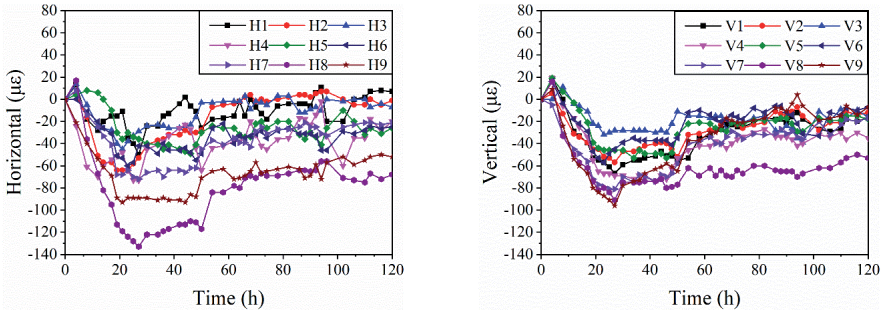

(a) horizontal strain (b) vertical strain

Fig. 3. Strain-time curve

It can be seen that the variation rules of vertical and horizontal strain-time curves of each point are similar. The maximum tensile strain occurs when the temperature difference between external and internal reaches the maximum value and is located at the centre of the specimen external. The three stages of temperature change still are used as the time interval for analyzing the strain variation rule. In stage I, the external temperature is low, but the internal temperature is high, leading to tension strain. With age development, the internal temperature increases and expands gradually, but confined by steel plates, bolts, and reinforcing bars, the specimen is subjected to compression. In stage II, due

to the difference in heat dissipation rate between external and internal, the maximum temperature difference appears, and the vertical and horizontal strains also reach the maximum value. As the specimen continues to cool down, the shrinkage of concrete restrained by steel plate, stud and reinforcing bars, and tensile strain appears. In stage III, the specimen is mainly subjected to compression, but the strain-time curve fluctuated. Some compressive strain converted to become tensile strain. During the whole process, the specimen's maximum tensile strain is $0.2*10^{-4}$, which is less than the concrete's ultimate tensile strain. That to say the specimen will not crack.

After five days of maintenance, the specimen formwork is removed, as shown in Fig. 4. No cracking is found on the surface of the specimen, which consistent with the strain analysis results. It indicates that for the SPCW with 400 mm thickness, the thermal stress caused by hydration heat in early stage will not cause cracking. The maintenance measures to prevent cracking in this test are appropriate. The reason for the cracking in previous corresponding projects may be attributed to improper maintenance or removing the formwork too early.

Fig. 4. Specimen after demoulding

3. FINITE ELEMENT ANALYSIS

3.1. FINITE ELEMENT MODEL

The temperature field and stress field caused by hydration heat were simulated using ANSYS and compared with the test results. In the thermal analysis, it can be concluded that the temperature change of reinforcing bars is synchronous with that of concrete, so it is neglected in the simulate process. A half finite element model of the specimen is established for the symmetry and the simplification calculation. The finite element model is shown in Fig. 5. The specimen thermal parameters are shown

in Table 2, τ is the time after concrete pouring. Due to the instability of the temperature field, the transient heat method is applied in heat transfer. The thermal-structural coupling field is selected for finite element analysis [14-15], thermal analysis is performed first, then transferred to structural analysis [16-17]. The solid70 element is selected as the steel plate, bolt and concrete for thermal analysis in the finite element model. This element has eight nodes, and each node has only one degree which can obtain good results for three-dimensional transient thermal analysis problems. When the thermal analysis is completed and transferred to the structural analysis, the element type would automatically convert to solid45. The total number of meshing elements were 192728. Only the temperature field generated by concrete hydration heat is considered in the analysis, and it is not affected by other external loads.

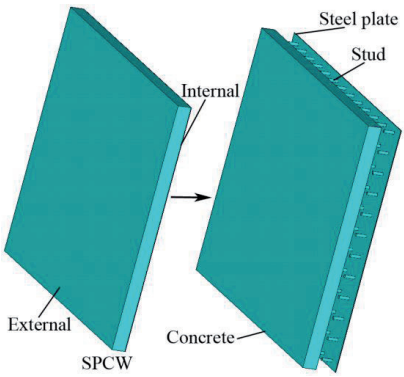

Fig. 5. Finite element model

Table 2. Calculation parameters of the specimen

Thermal parameters	Concrete	Steel	Unit
Density	2415.5	7850	kg/m^3
Heat conductivity	8.404	188	KJ/(m·h·C)
Heat emission coefficient	55	0	KJ/(m^2·h·C)
Specific heat capacity	0.95	0.48	KJ/kg
Heat of hydration	$330(1-e^{-0.69\tau^{0.56}})$	/	KJ/kg
Coefficient of thermal expansion	9e-6	12e-6	1/°C
Modulus of elasticity	$3.6e^4(1-e^{-0.28\tau^{0.52}})$	2.06e5	MPa
Poisson ratio	0.167	0.3	/

In the thermal analysis, the symmetry surface's heat emission coefficient (surface of steel) is 0 because it does not transfer heat, and the heat emission coefficient of the remaining three surfaces (surface concrete) is defined according to Table 2. The initial temperature of the atmospheric is set at 31 °C, which is the same as the experiment. In the stress field analysis, the boundary conditions were set up following the test's actual conditions, i.e., the top surface DOF is free while the other three surfaces were constrained. The load-time curve is divided into load steps to reflect the characteristics of load changing with time. The incremental time step is consistent with the test time (120 h), and the sub-step is 1.

3.2. FINITE ELEMENT RESULTS AND ANALYSIS

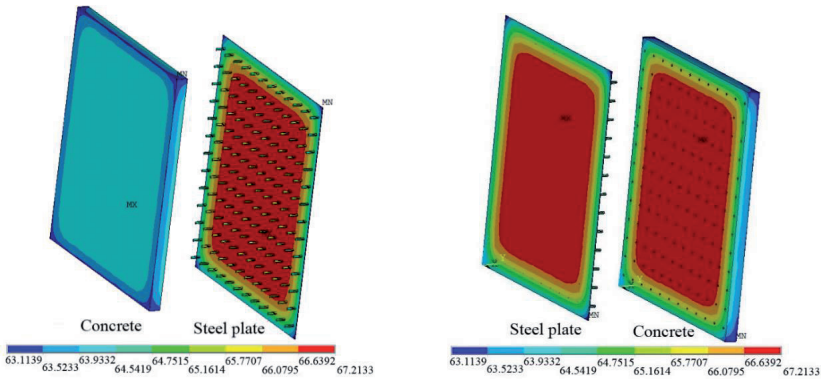

(a) specimen external (b) specimen internal

Fig. 6. Temperature contours of specimen

The specimen temperature contours at the maximum value are shown in Fig. 6. It can be seen that heat transfer is diffused from specimen internal to external. Internal temperature is higher than that of the external and the lowest temperature is at the four corners. The maximum temperature at the specimen external is 63.1°C and the specimen internal is 67.2°C. The steel plate is wrapped by concrete and forms a closed space in a small area, leading to heat concentration so that there is no difference between the temperature external and internal of the steel plate. Due to the changing trend of temperature results is similar to each point, the experimental results and finite element results at the centre of specimen external (T2) and internal (T7) are selected for comparative analysis. The comparison results were shown in Fig. 2. It can be seen that the time when the specimen reaches its maximum temperature, finite element result lags behind the experimental results by about 0.5 h, and

the maximum temperature difference between the two results is about 1.4 ºC. In the cooling stage, the decreasing rate of experimental results is faster than that of the finite element results. After 100 h, the finite element curve has a steady downward trend, while the experimental result has apparent fluctuation.

The temperature field's calculation results are extracted and then transferred to the structure field for structural analysis. When the tensile stress reaches the limit value of concrete, the SPCW will crack. So the results are extracted only the tensile stress of concrete in X-direction and Z-direction reach the maximum value. The calculation results are shown in Fig. 7, the compressive stress is positive and the tension stress is negative. It can be seen that the maximum tensile stress of concrete in X-direction is 0.167 MPa and in Z-direction is 0.117 MPa. The maximum tensile stress of concrete is much less than that of the limit value (3.6 MPa). It shows that the SPCW will not crack, which is consistent with the experimental results, and the finite element method can be used in the parametric analysis in the following sections.

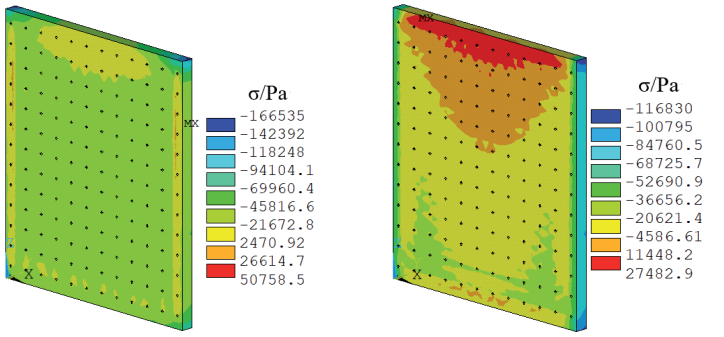

(a) stress contour in X direction (b) stress contour in Z direction

Fig. 7. Stress contour

4. PARAMETRIC ANALYSIS

4.1. CALCULATION RESULTS WITH DIFFERENT WALL THICKNESS

Based on experimental and finite element results of the SPCW with 400 mm thickness, the temperature field and stress field of 500 mm, 600 mm, 700 mm and 800 mm thickness walls were simulated by the finite element method. The calculation method, process, and material parameters are the same as 400 mm, only adjusted the wall's thickness. Temperature-time curves for the external and internal centre point of different thicknesses walls are shown in Fig. 8.

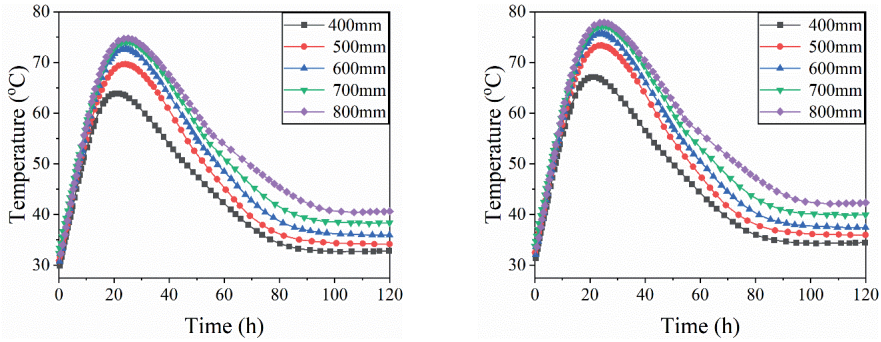

(a) external (b) internal

Fig. 8. Temperature-time curve of walls with different thicknesses

It can be seen that the temperature variation of the walls with five thicknesses shows a similar rule which increases sharply at first and then decreases slowly. When the heat production rate of concrete is equal to the external environment's convective heat transfer rate, the temperature reaches its peak value. No matter external or internal, the maximum temperature becomes high with the increase of thickness. When the wall thickness is 400 mm, the external and internal maximum temperature is 63.3 °C and 67.2 °C. When the wall thickness is 800 mm, the external and internal maximum temperature is 74.9 °C and 79.1 °C. For every 100 mm increase in wall thickness, the maximum temperature increases by about 3 °C, but the increased amplitude decreases gradually. With the increase of wall thickness, the time required for the maximum temperature becomes longer and longer. For the 400mm wall in the cooling stage, the curve tends to rise which shows that the atmospheric temperature greatly influences the wall temperature when the wall thickness is small.

4.2. CALCULATION RESULTS WITH DIFFERENT BOUNDARY CONDITION

The stress fields of different thickness SPCW with two-side (T) and four-side (F) connection constraints were analyzed, and stress-time curves for the external and internal centre point of different thicknesses walls are shown in Fig. 9. The tensile stress is positive and the compressive stress is negative. The 400-F mean that the 400 mm thickness wall is subject to four-side connection constraints, the 400-T mean that the 400 mm thickness wall is subject to two-side connection constraints, and other thicknesses are also expressed according to this method. The wall's temperature stress increases with the wall thickness increase, whether it is the two-side connection or the four-side connection constraints.

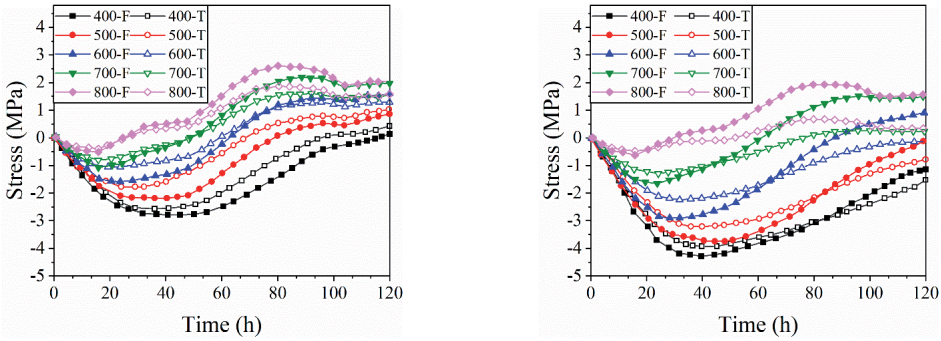

Fig. 9. Stress-time curve of walls with different thicknesses

From Fig 9 (a), it can be seen that on the external of the same thickness wall, the compressive stress with the four-side connection is greater than that with the two-side connection in the heating stage. In the cooling stage, when the wall thickness is more than 600mm, tensile stress with the four-side connection is greater than that with the two-side connection. When the wall thickness is less than 600mm, the tensile stress with the four-side connection is almost the same as that with the two-side connection. It indicates that atmospheric temperature has a significant influence on stress filed distribution of the small thickness SPCW in early stage of construction. From Fig 9 (b), it can be seen that on the internal of the same thickness wall, the compressive stress with four-side connection is greater than that with the two-side connection in the heating stage, and the tensile stress with four-side connection is also greater than that with the two-side connection in the cooling stage. The results show that using the two-side connection reduces the wall's external and internal stress levels and is conducive to preventing the wall cracking.

4.3. Calculation results with different steel plate thickness

The influence of different steel plate thickness on the deformation of SPCW is studied. In the analysis, the thickness of the walls is 400mm, while the thickness of steel plates (t) is 10mm, 15mm, 20mm, and 30mm, respectively. The analysis method and material properties are consistent with section 3, while the wall's boundary condition is constrained with the two-side connection. The analysis results of SPCW (concrete and steel plate) with different steel plate thickness when the displacement reaches the maximum value are shown in Fig. 10.

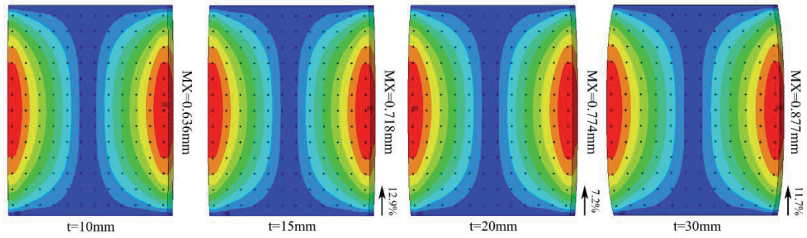

(a) displacement contour of the concrete

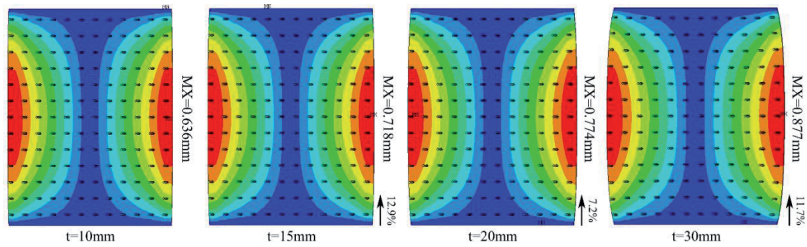

(b) displacement contour of the steel plate

Fig. 10. Displacement contour of SPCW with different steel plate thickness

It can be seen that due to the two-side connection, the wall deformation distribution characteristic is centrosymmetric along the wall length direction. The wall's top and bottom deformation are 0, and the closer to the wall top and bottom, the smaller the deformation. There is no constraint on the wall right and left sides, and the deformation is large, indicating that the constraint conditions have a significant influence on the deformation distribution characteristics. When the thickness of the steel plate is 10 mm, the maximum displacement of concrete and steel plate is 0.636 mm. When t=15 mm, the displacement increases by 12.9% compared with t=10 mm, t=20mm the displacement increases by 7.2% compared with t=15mm, t=30 mm the displacement increases by 11.7% compared with t=20 mm. It shows that with the increase of steel plate thickness, the steel plate and concrete deformation become generous, while the influence gradually decreases. For the same SPCW thickness, the deformation distribution character of steel plate and concrete is similar to each other, which indicates that the deformation coordination ability of these two materials is excellent. Moreover, the increase of the steel plate thickness does not change the deformation distribution character of the SPCW.

4.4. CALCULATION RESULTS WITH DIFFERENT STUD SPACE

The influence of different stud spaces on the SPCW deformation is studied. The walls' thickness is 400mm, while the stud space (d) is 200mm, 300mm, 400mm, and 500mm, respectively. The analysis

method and material properties are consistent with section 3, and the wall's boundary condition is also constrained with the two-side connection. The analysis results of SPCW (concrete and steel plate) with different stud spaces when the displacement reaches the maximum value are shown in Fig. 11.

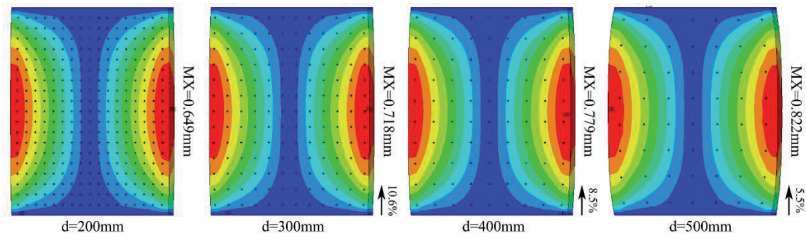

(a) displacement contour of the concrete

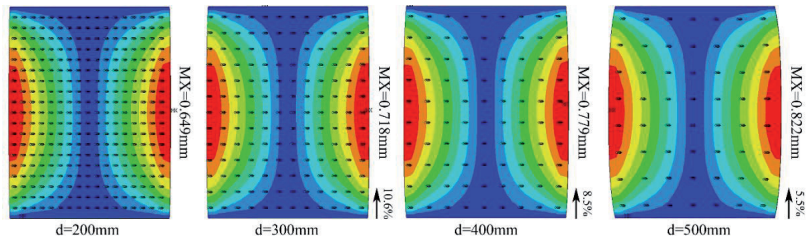

(b) displacement contour of the steel plate

Fig. 11. Displacement contour of SPCW with different stud space

It can be seen that the deformation of the wall distribution characteristic with different stud space is still centrosymmetric along the wall length direction due to the two-side connection. With the stud space increase, the steel plate and concrete deformation become generous. For the different stud space SPCW, the top and bottom sides' deformation is small, while the left and right sides are large. It indicates that the change of stud space does not change the deformation distribution character of the SPCW. When the wall stud space is 200 mm, the maximum displacement of concrete and steel plate is 0.649 mm. When d=300 mm, the displacement increases by 10.6% compared with d=200 mm, d=400mm the displacement increases by 8.5% compared with d=300mm, d=500 mm the displacement increases by 5.5% compared with d=400 mm. The SPCW stud space is small, the deformation of concrete and steel plate is also small, which indicates that the dense stud will lead the bond effect between concrete and steel plate be better and reduce the SPCW cracking.

From the above analyses, it can be seen that all the SPCW tensile stress values are less than the limit value of concrete tensile strength, which indicates that for SPCW with thickness less than 800mm, the thermal stress in the early stage of construction will not cause wall cracking. The SPCW with

small thickness is easily affected by the external atmosphere temperature, so moisture conservation measures should ensure that the hydration heat can be effectively dissipated after pouring. For the project with a longer construction period, the concrete with long design age can be selected to reduce the influence of hydration heat on the wall cracking. On the premise of satisfying the design strength, the steel plate wall with dense studs and small thickness can be selected to reduce the influence of incompatible deformation between steel plate and concrete to avoid the wall cracking.

5. CONCLUSION

Based on the physical testing and the finite element analysis results, the behaviour of the small thickness SPCW could be summarized as,

1. For 400 mm thickness SPCW, there is a massive temperature difference between the external and internal in the early stage of construction, which causes tensile stress. However, the tensile stress is far less than the cracking stress, and there is no crack on the surface of the wall in the test.
2. With the increase of wall thickness, the time required to reach the maximum temperature becomes longer and longer, which indicates that large thickness SPCW may need longer maintenance time, and for the long construction period project, the concrete with long design age can be selected to reduce the influence of hydration heat on the wall cracking.
3. For SPCW with thickness less than 800mm, the temperature stress caused by hydration heat in the early stage of construction is small, and the wall will not crack.
4. The wall thickness, steel plate thickness, boundary condition, and stud space significantly influence the temperature field and stress field distribution on the small thickness SPCW in the early stage of construction, and reasonable maintenance measures can avoid cracking.

REFERENCES

1. H.S. Hu, J.G. Nie, M.R. Eatherton, "Deformation capacity of concrete-filled steel plate composite shear walls", Journal of Constructional Steel Research 103:148-158, 2014.
2. J.J. Wang, M.X. Tao, J.S. Fan, X. Nie, "Seismic Behavior of Steel Plate Reinforced Concrete Composite Shear Walls under Tension-Bending-Shear Combined Cyclic Load", Journal of Structural Engineering 144: 2018.
3. S. Epackachi, A.S. Whittaker, A. Aref, "Seismic analysis and design of steel-plate concrete composite shear wall piers", Engineering structure 133: 105-123, 2017.
4. K.J. Lee, K.M. Hwang, K.W. Hahm, S.T. Yi, "Shear strength of joints between reinforced concrete slabs and steel-plate-concrete walls", Proceedings of the Institution of Civil Engineers-Structures and Buildings 171: 739-754, 2018.
5. N.H. Nguyen, A.S. Whittaker, "Numerical modelling of steel-plate concrete composite shear walls", Engineering structure 150: 1-11, 2017.

6. W. Wang, Y. Wang, Z. Lu, "Experimental study on seismic behavior of steel plate reinforced concrete composite shear wall", Engineering structure 160: 281-292, 2018.
7. D.Y. Yoo, J.J. Park, S.W. Kim, Y.S. Yoon, "Influence of reinforcing bar type on autogenous shrinkage stress and bond behavior of ultra high performance fiber reinforced concrete", Cement & Concrete Composites 48: 150-161, 2014.
8. X.J. Gao, G.B. Qu, A.L. Zhang, "Influences of reinforcement on differential drying shrinkage of concrete", Journal of Wuhan University of Technology-Materials Science Edition 27: 576-580, 2012.
9. L. Zeng, "Research on early-age crack control of steel plate concrete composite shear wall", Chongqing University, Master's thesis, China, 2013.
10. L.P. Huang, J.M. Hua, M. Kang, Q.M. Luo, F.B. Zhou, "Influence of Steel Plates and Studs on Shrinkage Behavior and Cracking Potential of High-Performance Concrete", Materials 12: 2019.
11. L.P. Huang, J.M. Hua, M. Kang, A.L. Zhang, "Influence of reinforcement configuration on the shrinkage and cracking potential of high-performance concrete", Construction and Building Materials 140: 20-30, 2017.
12. X.J. Wang, P.P. Cai, X.B. Zhang, W, Lu, "Experimental study on early temperature field of large thickness composite shear wall", Sichuan Building Science 44: 57-62, 2018.
13. X.X. Gu, "Research on early-age cracks of high-strength mass concrete in steel plate-concrete composite shear wall", Tianjin University, Master's thesis, China, 2015.
14. G. Bertagnoli, G. Mancini, F. Tondolo, "Numerical modelling of early-age concrete hardening", Magazine of Concrete Research 61: 299-307, 2009.
15. X.Y. Wang, H.K. Cho, H.S. Lee, "Prediction of temperature distribution in concrete incorporating fly ash or slag using a hydration model", Composites Part B-Engineering 42: 27-40, 2011.
16. B.J. Sun, X.R. Wang, Z.Y. Wang, Y.H. Gao, "Transient temperature calculation method for deep-water cementing based on hydration kinetics model", Applied Thermal Engineering 129: 1426-1434, 2018.
17. S. Swaddiwudhipong, D. Chen, M.H. Zhang, "Simulation of the exothermic hydration process of Portland cement", Advances in Cement Research 14: 61-69, 2002.

LIST OF FIGURES AND TABLES:

Received: 19.08.2020, Revised: 07.11.2020